Nonlinear theory of index enhancement via quantum coherence and interference

U. Rathe, M. Fleischhauer, and Shi-Yao Zhu
Department of Physics, Texas A&M University, College Station, Texas 77843

T. W. Hänsch and M. O. Scully
Max-Planck-Institut für Quantenoptik, 8046 Garching, Germany
(Received 4 August 1992)

We study the nonlinear behavior of the electric susceptibility for several systems showing a high index of refraction without absorption due to quantum coherence and interference. Estimates of cw intensity limits for a given index of refraction are obtained. We calculate critical field intensities for self-focusing and investigate the stability of the absorption cancellation with regard to intensity fluctuations.

PACS number(s): 42.65.An, 42.50.Md, 42.65.Hw, 42.50.Hz

I. INTRODUCTION

Quantum coherence and interference in atomic systems can lead to interesting optical phenomena such as nonabsorbing resonances [1–3] and lasing without inversion [4–7]. Recently it has been proposed to exploit atomic coherence and interference to generate an ultrahigh index of refraction without absorption [8–10]. For this effect, several coherence-establishing schemes have been investigated [11]. However, results were obtained only for the linear response of the medium [12]. But as the effect takes place in the vicinity of an atomic resonance, large nonlinearities are to be expected and need to be taken into account for potential applications of high-index materials, in particular if large field amplitudes are required as in the example of a laser accelerator [13].

With increasing probe-field amplitudes the susceptibility $\chi(\omega)$ of the medium, which describes the response to a probe field with frequency ω, becomes dependent on the intensity

$$\chi(\omega,E)=\chi^{(1)}(\omega)+\chi^{(3)}(\omega)|E|^2+\chi^{(5)}(\omega)|E|^4+\cdots . \quad (1)$$

The higher-order terms in Eq. (1) lead to a saturation of the total polarization with increasing intensity $|E|^2$, which in turn affects the utilization of nonabsorbing media with an ultrahigh index of refraction in essentially three ways.

First, in the limit of strong probe fields the saturation of the polarization reduces the maximum achievable index of refraction for a given density of atoms.

Second, in most of the systems discussed in Refs. [8–11], the high index with vanishing absorption occurs at a frequency $\omega=\omega_0$ that is the transition point from an absorption to a gain region. A change in the field intensity can shift the frequency ω_0 of zero absorption so that the system will eventually display absorption or gain. If an increase of the input intensity leads to gain, the system is unstable since fluctuations of the input intensity are amplified.

The third question of interest arises when we go from the idealized plane-wave picture to a more realistic description that includes the beam profile. Then the intensity dependence of the index of refraction may lead to self-focusing and eventually to the destruction of the material.

In the present paper we give the full nonlinear results for the susceptibility for three different coherence schemes, namely the initial coherence scheme [8], the microwave scheme [9], and the Raman scheme [11], and analyze the nonlinearities with respect to the three problems stated above. In Sec. II we derive a limit for the maximum achievable index of refraction for a given density of atoms and a given probe-field amplitude. In Sec. III we calculate the critical field intensity for self-focusing, and in Sec. IV we examine the stability of the systems with respect to intensity fluctuations.

II. NONLINEAR LIMITS FOR THE INDEX OF REFRACTION

In this section we investigate the maximum achievable index of refraction for the three schemes mentioned in the Introduction for the case of a cw single-mode probe field of given intensity.

A qualitative limit for this quantity can be derived easily from the microscopic definition of the total polarization P in a two-level system

$$P=N\not{\mu}\rho_{ab} , \quad (2)$$

where N is the atomic number density, $\not{\mu}$ is the electric dipole matrix element of the optical transition $|a\rangle\rightarrow|b\rangle$, and ρ_{ab} is the corresponding matrix element of the density matrix. The absolute value of ρ_{ab} is always smaller than unity, and the dipole matrix element can reach values of the order of a_0e, where a_0 is the Bohr radius and e is the elementary charge. Therefore P is limited by $P\lesssim Na_0e$, so that we have, for a given field amplitude E, a limit for the real part of the susceptibility χ' at a point of vanishing absorption ($\chi''=0$)

$$\chi'\lesssim\frac{Na_0e}{\epsilon_0E} . \quad (3)$$

Here we have used $P=\epsilon_0\chi'E$. As an example, for

$N=10^{22}\ m^{-3}$ and $E=10^{9}$ V m^{-1}, which are typical numbers in a laser accelerator, χ' is limited by

$$\chi' \lesssim 10^{-5} . \tag{4}$$

This result establishes an approximate upper bound for the index of refraction $n \equiv \sqrt{1+\chi'}$ regardless of the specifics of the system under discussion. The *actual* saturation behavior of systems with vanishing absorption is the problem addressed in the following sections.

A. Initial coherence scheme

In the initial coherence case, we consider three-level atoms which are injected into the interaction region after being prepared in a coherent superposition of the two lower levels $|b\rangle$ and $|b'\rangle$ [see Fig 1(a)] [8]. This can be achieved, for example, by excitation of the atoms from a lower level with a coherent pulse at a time just before the atoms enter the interaction region.

If we introduce the atomic injection rate r and use the technique described in Ref. [14] to sum over all atoms, we obtain the equations of motion for the total matrix in a rotating frame

$$\dot{\rho}_{aa} = r\rho^0_{aa} - \gamma_a \rho_{aa} - \frac{i}{\hbar}[(\not{\mu}'\rho_{b'a} + \not{\mu}\rho_{ba})E - \text{c.c.}] , \tag{5}$$

$$\dot{\rho}_{bb} = r\rho^0_{bb} - \gamma_b \rho_{bb} - \frac{i}{\hbar}(\not{\mu}\rho_{ab}E^* - \text{c.c.}) , \tag{6}$$

$$\dot{\rho}_{b'b'} = r\rho^0_{b'b'} - \gamma_{b'}\rho_{b'b'} - \frac{i}{\hbar}(\not{\mu}'\rho_{ab'}E^* - \text{c.c.}) , \tag{7}$$

$$\dot{\rho}_{ab} = -(\gamma_{ab} + i\Delta_{ab})\rho_{ab} - \frac{i}{\hbar}\not{\mu}(\rho_{bb} - \rho_{aa})E - \frac{i}{\hbar}\not{\mu}'\rho_{b'b}E , \tag{8}$$

$$\dot{\rho}_{ab'} = -(\gamma_{ab'} + i\Delta_{ab'})\rho_{ab'} - \frac{i}{\hbar}\not{\mu}'(\rho_{b'b'} - \rho_{aa})E - \frac{i}{\hbar}\not{\mu}\rho_{bb'}E , \tag{9}$$

$$\dot{\rho}_{b'b} = r\rho^0_{b'b} - (\gamma_{b'b} + i\omega_{b'b})\rho_{b'b} - \frac{i}{\hbar}(\not{\mu}'\rho_{ab}E^* - \not{\mu}\rho_{b'a}E) . \tag{10}$$

Here ρ^0 is the initial density matrix of an individual injected atom, E is the slowly varying amplitude of the probe field, $\not{\mu}$ and $\not{\mu}'$ denote the (real) dipole matrix elements of the transition $|b\rangle \rightarrow |a\rangle$ and $|b'\rangle \rightarrow |a\rangle$, respectively, and $\Delta_{\alpha\beta} = \omega_{\alpha\beta} - \nu$ with ν being the probe-field frequency. r, γ_a, γ_b, $\gamma_{b'}$ are the decay and pump rates depicted in Fig. 1(a).

We solve the corresponding liner system of algebraic equations analytically in the steady state. For the susceptibility defined by

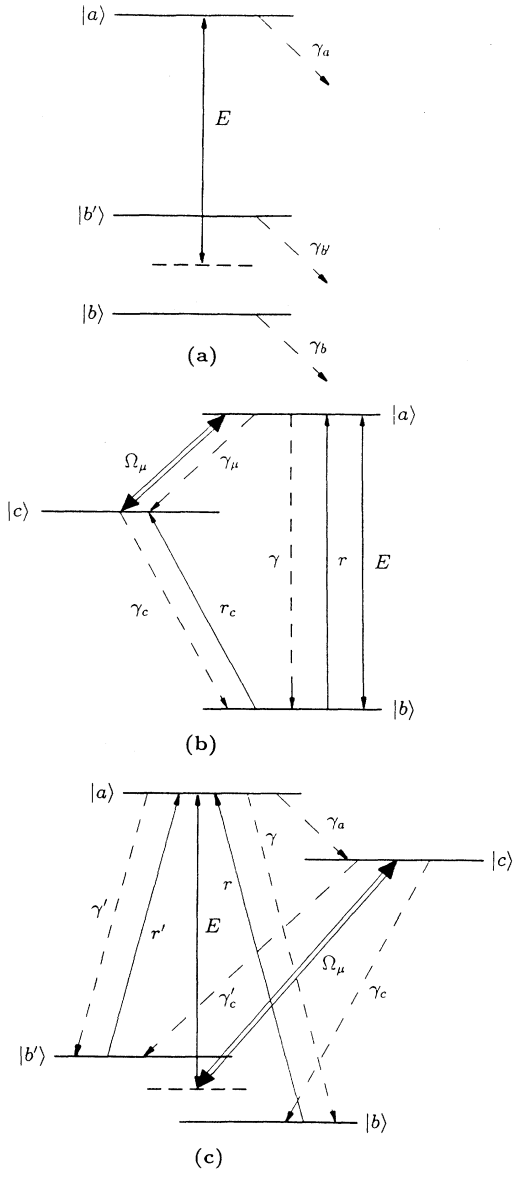

FIG. 1. Level schemes for the three discussed systems. (a) Initial coherence scheme, (b) microwave driven Λ scheme, and (c) Raman driven scheme.

$$\chi \equiv \chi' + i\chi'' = -\frac{(\not{\mu}\rho_{ab} + \not{\mu}'\rho_{ab'})}{\epsilon_0 V E} , \tag{11}$$

where E is the probe field and V is the interaction volume, we obtain for the simplified case with $\not{\mu}' = \not{\mu}$, $\gamma_{b'} = \gamma_b$ and equal initial populations of the levels $|b\rangle$ and $|b'\rangle$ $[\rho^0_{bb} = \rho^0_{b'b'} = (1-\rho^0_{aa})/2]$

$$\chi = \frac{\not{\mu}^2}{\epsilon_0 \hbar V}\frac{r}{2}\frac{(A'+B'|\Omega|^2+C'|\Omega|^4)+i(A''+B''|\Omega|^2+C''|\Omega|^4)}{a+b|\Omega|^2+c|\Omega|^4+d|\Omega|^6} , \tag{12}$$

where $\Omega = \not{\mu}E/\hbar$ and the real coefficients $A'', B'', C'', a, b, c, d$ depend only on the system parameters:

$$A' = 2\Delta\gamma_b\{a_1 a_3 R_0 + 2\gamma_a\gamma_b[(a_1\gamma_b - \gamma_{ab}\omega^2_{b'b})\text{Re}(\rho^0_{b'b}) + \omega_{b'b}(a_1 + \gamma_{ab}\gamma_b)\text{Im}(\rho^0_{b'b})]\} , \tag{13}$$

$$A''=2\gamma_b(a_2a_3\gamma_{ab}R_0+2\gamma_a\gamma_b\{[a_2(\gamma_{ab}\gamma_b-\omega_{b'b}^2/2)+\Delta^2\omega_{b'b}^2]\mathrm{Re}(\rho_{b'b}^0)+\omega_{b'b}[a_2(\gamma_{ab}+\gamma_b/2)-\Delta^2\gamma_b]\mathrm{Im}(\rho_{b'b})\}) , \quad (14)$$

$$B'=4\Delta\{[2\gamma_b^2\gamma_{ab}+\omega_{b'b}^2(\gamma_{ab}+\gamma_b/2)]R_0+\gamma_b[4\gamma_{ab}(\gamma_a\gamma_b-\omega_{b'b}^2)\mathrm{Re}(\rho_{b'b}^0)+\omega_{b'b}(4\gamma_a\gamma_b+2\gamma_b^2+\gamma_a^2)\mathrm{Im}(\rho_{b'b}^0)]\} , \quad (15)$$

$$B''=[8\gamma_{ab}^2\gamma_b^2+\omega_{b'b}^2(4\gamma_{ab}^2+\gamma_b^2)]R_0+4\gamma_a\gamma_b[(4\gamma_{ab}^2\gamma_b-\omega_{b'b}^2\gamma_a/2)\mathrm{Re}(\rho_{b'b}^0)+2\omega_{b'b}\gamma_{ab}(\gamma_{ab}+\gamma_b/2)\mathrm{Im}(\rho_{b'b}^0)] , \quad (16)$$

$$C'=8\Delta\gamma_b[R_0+2\gamma_a\mathrm{Re}(\rho_{b'b}^0)] , \quad (17)$$

$$C''=8\gamma_b\gamma_{ab}[R_0+2\gamma_a\mathrm{Re}(\rho_{b'b}^0)] , \quad (18)$$

$$a=a_3\gamma_a\gamma_b^2[\gamma_{ab}^2+(\Delta+\omega_{b'b}/2)^2][\gamma_{ab}^2+(\Delta-\omega_{b'b}/2)^2] , \quad (19)$$

$$b=-2\gamma_b[\gamma_a\gamma_b\omega_{b'b}^2(\gamma_{ab}^2-\Delta^2+\omega_{b'b}^2/4)-2a_2\gamma_{ab}(2a_3\gamma_{ab}+\gamma_a\gamma_b^2)] , \quad (20)$$

$$c=-2\gamma_{ab}[-2\gamma_b^2\gamma_{ab}(5\gamma_a+4\gamma_b)-\omega_{b'b}^2(\gamma_a^2+\gamma_a\gamma_b+4\gamma_b^2)]+4\Delta^2\gamma_a\gamma_b^2 , \quad (21)$$

$$d=32\gamma_b\gamma_{ab}^2 , \quad (22)$$

and

$$\begin{aligned} R_0&=\gamma_a-(\gamma_a+2\gamma_b)\rho_{aa}^0 ,\\ a_1&=\gamma_{ab}^2+\Delta^2-\omega_{b'b}^2/4 ,\\ a_2&=\gamma_{ab}^2+\Delta^2+\omega_{b'b}^2/4 ,\\ a_3&=\gamma_b^2+\omega_{b'b}^2 ,\\ \Delta&=\Delta_{ab}-\omega_{b'b}/2\equiv\Delta_{ab'}+\omega_{b'b}/2 . \end{aligned} \quad (23)$$

The real and imaginary parts of the resulting susceptibility χ' and χ'' are plotted in Fig. 2 for different probe-field amplitudes. From numerical calculations we find that the susceptibility corresponds to that of the linear analysis if the Rabi frequency Ω is small compared to the decay rates of the optical polarization, i.e., to the decay rates of the nondiagonal elements ρ_{ab} and $\rho_{ab'}$. For higher field intensities, however, the maxima of χ' decrease.

The imaginary part of χ [see Fig. 2(b)], which drives the amplitude of the field, shows a zero at a transition point from an absorption region ($\chi''>0$) to a gain region ($\chi''<0$). We draw attention to the fact that the nonlinearities do not only lead to saturation as in the case of χ', but also to a shift of the detuning of vanishing absorption. This will turn out to be important for the stability of the systems and shall be discussed further in Sec. IV.

We discuss the results for the nonlinear susceptibilities in view of the application of the high index material to a laser accelerator [13]. For this application, two objectives have to be met. First, a high probe field is necessary to achieve a large energy gain in the acceleration process. Second, we need a sufficient index of refraction to slow down the phase velocity of the wave while the density of the gas should be kept as low as possible to avoid scattering of the charged particles.

We recognize from Eq. (12) that the nonlinear contributions to the susceptibility are at least second order in the Rabi frequency. Hence the product of χ' and $|\Omega|$ has a maximum, for which we estimate by testing different system parameters

$$\chi'\frac{|\Omega|}{\gamma}\lesssim 5\times10^{-16}N\ \mathrm{cm}^3 . \quad (24)$$

Here N is the atomic number density $N=r/(\gamma V)$.

To see the impact of these results on the application of the laser accelerator we now consider a specific numerical example. For a typical value of the allowed atomic number density N of 2×10^{22} m^{-3}, corresponding to a pres-

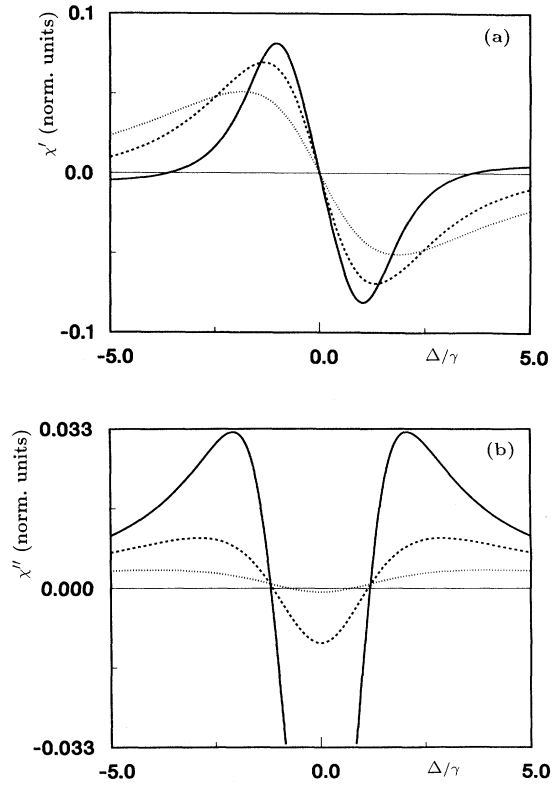

FIG. 2. (a) Real and (b) imaginary part of the susceptibility in normalized units as functions of the detuning for the initial coherence scheme. Plotted is $\chi[\wp^2r/(\epsilon_0\hbar\gamma^2V)]^{-1}$. Note that in our formalism the atomic number density is given by $N=r/\gamma V$ with the cavity volume V. The parameters are $\gamma_a=0.1\gamma,\gamma_b=\gamma_{b'}=2\gamma,\omega_{b'b}=2\gamma,\rho_{aa}^0=0.01$, $\rho_{bb}^0=\rho_{b'b'}^0=0.495$, $\rho_{b'b}^0=-i0.495$. The three curves correspond to field amplitudes of $\Omega=0.1\gamma$ (solid); 0.5γ (dashed); γ (dotted). (The parameters used for this system are the same as in Ref. [8].)

sure of 1 Torr at room temperature, a wavelength of $\lambda=500$ nm, and a decay rate $\gamma=10^8\ \mathrm{s}^{-1}$, we find that the maximum probe field amplitude for the required χ' of 10^{-5} is of order $10^8\ \mathrm{V\,m}^{-1}$.

B. Microwave driven Λ scheme

In this closed atomic scheme the atomic coherence is maintained by a strong microwave field that couples the upper level of the probe-field transition $|a\rangle\rightarrow|b\rangle$ to an auxiliary level $|c\rangle$ [see Fig. 1(b)]. In the following equations of motion for the density matrix we have included indirect pumping mechanisms with rates r and r_c:

$$\dot\rho_{aa}=-(\gamma+\gamma_\mu)\rho_{aa}+r\rho_{bb}-i\left[\frac{\not{E}}{\hbar}\rho_{ba}+\Omega_\mu\rho_{ca}-\text{c.c.}\right], \tag{25}$$

$$\dot\rho_{bb}=\gamma\rho_{aa}-(r+r_c)\rho_{bb}+\gamma_c\rho_{cc}+i\left[\frac{\not{E}}{\hbar}\rho_{ba}-\frac{\not{E}^*}{\hbar}\rho_{ab}\right], \tag{26}$$

$$\dot\rho_{cc}=\gamma_\mu\rho_{aa}+r_c\rho_{bb}-\gamma_c\rho_{cc}+i(\Omega_\mu\rho_{ca}-\Omega_\mu^*\rho_{ac}), \tag{27}$$

$$\dot\rho_{ab}=-(i\Delta+\gamma_{ab})\rho_{ab}+i\frac{\not{E}}{\hbar}(\rho_{aa}-\rho_{bb})-i\Omega_\mu\rho_{cb}, \tag{28}$$

$$\dot\rho_{cb}=-[i(\Delta-\Delta_\mu)+\gamma_{cb}]\rho_{cb}-i\Omega_\mu^*\rho_{ab}+i\frac{\not{E}}{\hbar}\rho_{ca}, \tag{29}$$

$$\dot\rho_{ac}=-(i\Delta_\mu+\gamma_{ac})\rho_{ac}+i\Omega_\mu(\rho_{aa}-\rho_{cc})-i\frac{\not{E}}{\hbar}\rho_{bc}. \tag{30}$$

Here we have used $\Delta=\omega_{ab}-\nu$ with the probe frequency ν, $\Delta_\mu=\omega_{ac}-\nu_\mu$ with the microwave frequency ν_μ, the Rabi frequency of the microwave field Ω_μ, the slowly varying amplitude of the probe field E, the dipole matrix element of the optical transition $\not{}$, and the pump and decay parameters $\gamma,\gamma_\mu,\gamma_c,r$, and r_c according to Fig. 1(b). Again this system is solved analytically in the steady state. For the susceptibility defined by

$$\chi=-\frac{\not{N}\rho_{ab}}{\epsilon_0 E}, \tag{31}$$

we find in the simplified case $\gamma_\mu=r=\Delta_\mu=0$

$$\chi=-\frac{N\not{}^2}{\epsilon_0\hbar}\frac{(A'+B'|\Omega|^2+C'|\Omega|^4)+i(A''+B''|\Omega|^2+C''|\Omega|^4)}{a+b|\Omega|^2+c|\Omega|^4+d|\Omega|^6}, \tag{32}$$

where the coefficients $A',B',C',A'',B'',C'',a,b,c$, and d are given by

$$A'=\Delta\gamma_{ac}\{(\gamma_{cb}^2+\Delta^2-|\Omega_\mu|^2)[-\gamma_{ac}(\gamma\gamma_c+4|\Omega_\mu|^2)+2r_c|\Omega_\mu|^2]+\gamma r_c|\Omega_\mu|^2(\gamma_{ab}+\gamma_{cb})\}, \tag{33}$$

$$A''=\gamma_{ac}\{a_2[-\gamma_{ac}(\gamma\gamma_c+4|\Omega_\mu|^2)+2r_c|\Omega_\mu|^2]+\gamma r_c|\Omega_\mu|^2(-\Delta^2+\gamma_{ab}\gamma_{cb}+|\Omega_\mu|^2)\}, \tag{34}$$

$$B'=\Delta\{-2\gamma_{ac}[\gamma_c(\gamma\gamma_{cb}+|\Omega_\mu|^2)+2\gamma_{cb}|\Omega_\mu|^2]+r_c|\Omega_\mu|^2(4\gamma_{ac}+r_c)\}, \tag{35}$$

$$B''=-\gamma_{ac}[2\gamma_{ab}\gamma_{cb}(\gamma\gamma_c+2|\Omega_\mu|^2)+\gamma\gamma_c|\Omega_\mu|^2]+r_c\gamma_{ab}|\Omega_\mu|^2(\gamma+2\gamma_{cb}), \tag{36}$$

$$C'=-\Delta\gamma\gamma_c, \tag{37}$$

$$C''=-\gamma\gamma_c\gamma_{ab}, \tag{38}$$

$$a=\gamma_{ac}[(\Delta^2-|\Omega_\mu|^2)^2+\Delta^2(\gamma_{ab}^2+\gamma_{cb}^2)+\gamma_{ab}\gamma_{cb}(\gamma_{ab}\gamma_{cb}+2|\Omega_\mu|^2][2\gamma\gamma_{ac}\gamma_{cb}+4|\Omega_\mu|^2(\gamma_{ac}+r_c)], \tag{39}$$

$$b=2\{a_1a_2\gamma_{ac}^2+a_3[2\gamma\gamma_{ac}\gamma_{cb}+(\gamma_c+2r_c)|\Omega_\mu|^2]+6\gamma_{ac}\Delta^2|\Omega_\mu|^2(\gamma_{cb}+\gamma_{ab})+\gamma|\Omega_\mu|^2[\Delta^2(\gamma_{cb}-\gamma_{ac})+(\gamma_{ab}+\gamma_{ac})(\gamma_{cb}\gamma_{ab}+|\Omega_\mu|^2)]\}, \tag{40}$$

$$c=2\gamma a_3+2\gamma_{ac}a_1(2\gamma_{ab}\gamma_{cb}+|\Omega_\mu|^2), \tag{41}$$

$$d=2\gamma_{ab}a_1, \tag{42}$$

with

$$a_1=2\gamma_c+r_c,\quad a_2=\gamma_{ab}(\Delta^2+\gamma_{cb}^2)+\gamma_{cb}|\Omega_\mu|^2,\quad a_3=\gamma_{cb}(\Delta^2+\gamma_{ab}^2)+\gamma_{ab}|\Omega_\mu|^2. \tag{43}$$

The resulting susceptibility is plotted for different intensities in Fig. 3. We see similar effects as in the initial coherence scheme and stress the fact that χ' also decreases at the point of zero absorption, as seen for the initial coherence scheme. An estimate for the limit of the product χ' and $|\Omega|$ is

$$\frac{|\Omega|}{\gamma}\chi'\lesssim 10^{-15}N\ \mathrm{cm}^3. \tag{44}$$

Using the same parameters as in the example in Sec. II A, relevant to the laser accelerator, we here find a maximum field amplitude of order $10^9\ \mathrm{V\,m}^{-1}$.

C. Raman driven scheme

In the Raman driven scheme coherence between two lower levels $|b\rangle$ and $|b'\rangle$ is established via a coupling to an auxiliary level $|c\rangle$ by a strong coherent driving field [see Fig. 1(c)]. The equations of motion for the density

matrix in a rotating frame read

$$\dot{\rho}_{aa}=-(\gamma+\gamma'+\gamma_a)\rho_{aa}+r\rho_{bb}+r'\rho_{b'b'} +i\left[\frac{\wp}{\hbar}E^*\rho_{ab}+\frac{\wp'}{\hbar}E^*\rho_{ab'}-\text{c.c.}\right], \tag{45}$$

$$\dot{\rho}_{b'b'}=-(\gamma'_b+r')\rho_{b'b'}+\gamma_b\rho_{bb}+\gamma'\rho_{aa}+\gamma'_c\rho_{cc} +i\left[\frac{\wp'}{\hbar}E\rho_{b'a}+\Omega'_R\rho_{b'c}-\text{c.c.}\right], \tag{46}$$

$$\dot{\rho}_{bb}=-(\gamma_b+r)\rho_{bb}+\gamma'_b\rho_{b'b'}+\gamma\rho_{aa}+\gamma_c\rho_{cc} +i\left[\frac{\wp}{\hbar}E\rho_{ba}+\Omega_R\rho_{bc}-\text{c.c.}\right], \tag{47}$$

$$\dot{\rho}_{cc}=-(\gamma_c+\gamma'_c)\rho_{cc}+\gamma_a\rho_{aa} +i(\Omega'^*_R\rho_{cb'}+\Omega^*_R\rho_{cb}-\text{c.c.}), \tag{48}$$

$$\dot{\rho}_{ab'}=-(\gamma_{ab'}+i\Delta_{ab'})\rho_{ab'} +i\left[\frac{\wp'}{\hbar}E(\rho_{aa}-\rho_{b'b'})-\frac{\wp}{\hbar}E\rho_{bb'}+\Omega'_R\rho_{ac}\right], \tag{49}$$

$$\dot{\rho}_{ab}=-(\gamma_{ab}+i\Delta_{ab})\rho_{ab} +i\left[\frac{\wp}{\hbar}E(\rho_{aa}-\rho_{bb})-\frac{\wp'}{\hbar}E\rho_{b'b}+\Omega_R\rho_{ac}\right], \tag{50}$$

$$\dot{\rho}_{b'b}=-[\gamma_{b'b}+i(\Delta_{ab}-\Delta_{ab'})]\rho_{b'b} +i\left[\frac{\wp}{\hbar}E\rho_{b'a}-\frac{\wp'}{\hbar}E^*\rho_{ab}+\Omega_R\rho_{b'c}-\Omega'^*_R\rho_{cb}\right], \tag{51}$$

$$\dot{\rho}_{cb'}=-(\gamma_{cb'}+i\Delta'_R)\rho_{cb'} +i\left[\Omega'_R(\rho_{cc}-\rho_{b'b'})-\Omega_R\rho_{bb'}+\frac{\wp'}{\hbar}E\rho_{ca}\right], \tag{52}$$

$$\dot{\rho}_{cb}=-(\gamma_{cb}+i\Delta_R)\rho_{cb} +i\left[\Omega_R(\rho_{cc}-\rho_{bb})-\Omega'_R\rho_{b'b}+\frac{\wp}{\hbar}E\rho_{ca}\right], \tag{53}$$

$$\dot{\rho}_{ac}=-[\gamma_{ac}+i(\Delta_{ab}-\Delta_R)]\rho_{ac} -i\left[\frac{\wp}{\hbar}E\rho_{bc}+\frac{\wp'}{\hbar}E\rho_{b'c}-\Omega^*_R\rho_{ab}-\Omega'^*_R\rho_{ab'}\right]. \tag{54}$$

Here we have used $\Delta_{ab}=\omega_{ab}-\nu$ and $\Delta_R=\omega_{cb}-\nu_R$ with the frequency of the driving field ν_R and the dipole matrix element $\wp$ of the optical transition $|a\rangle\rightarrow|b\rangle$. Ω_R is the Rabi frequency of the driving field, $\gamma,\gamma_a,\gamma_b,\gamma_c$, and r are the decay and pump parameters according to Fig. 1(c), and all corresponding quantities for the transition $|a\rangle\rightarrow|b'\rangle$ are indicated by primes.

The steady-state solutions were obtained numerically, leading to susceptibilities as plotted in Figs. 4 and 5.

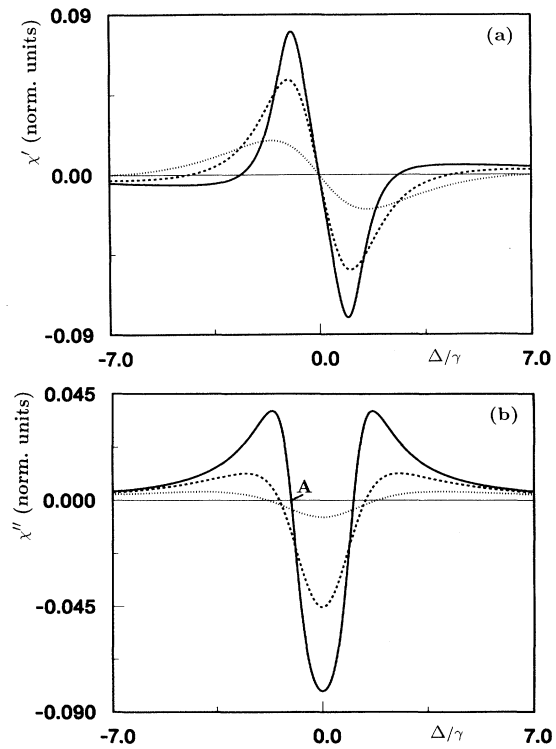

FIG. 3. (a) Real and (b) imaginary part of the susceptibility in normalized units as functions of the detuning for the upper level microwave scheme. Plotted is $\chi[N\wp^2/(\epsilon_0\hbar\gamma)]^{-1}$. The parameters are $\gamma_c=0.1\gamma$, $\Omega_\mu=\gamma$, $r_c=\gamma$, $\gamma_\mu=r=0$. The three curves correspond to field amplitudes of $\Omega=0.1\gamma$ (solid); γ (dashed); 2γ (dotted).

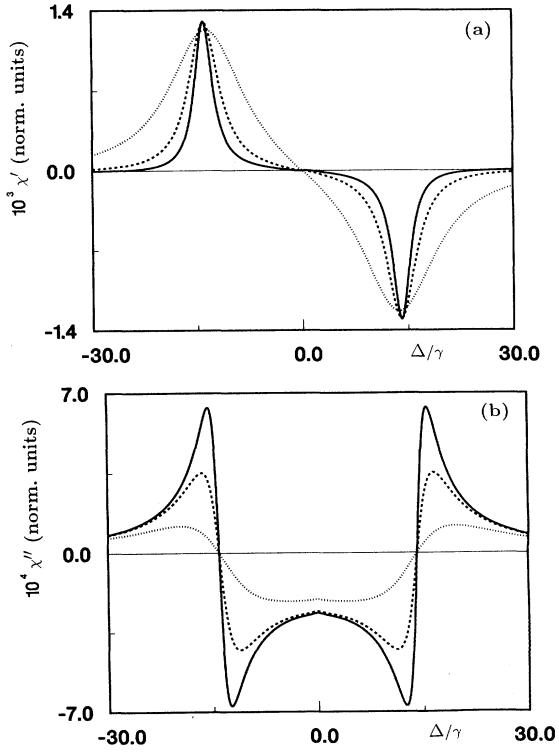

FIG. 4. (a) Real and (b) imaginary part of the susceptibility in normalized units (see Fig. 3) as functions of the detuning for the Raman driven scheme. The parameters are $\gamma_a=\gamma_b=\gamma_{b'}=10^{-3}\gamma$, $\gamma_c=\gamma$, $\omega_{b'b}=\gamma$, $\Omega_R=10\gamma$, $r=0.06\gamma$. The three curves correspond to field amplitudes of $\Omega=0.1\gamma$ (solid); γ (dashed); 3γ (dotted).

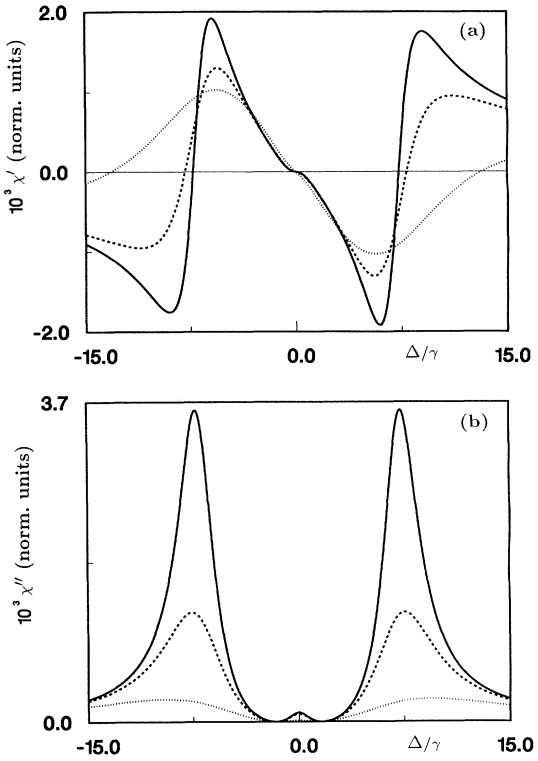

FIG. 5. (a) Real and (b) imaginary part of the susceptibility in normalized units as functions of the detuning for the Raman driven scheme with adjusted pump parameter. Note the spectral region of small absorption. The parameters are $\gamma_a=\gamma_b=\gamma_{b'}=10^{-3}\gamma$, $\gamma_c=\gamma$, $\omega_{b'b}=\gamma$, $\Omega_R=5\gamma$. The three curves correspond to field amplitudes of $\Omega=0.1\gamma$ (solid); γ (dashed); 3γ (dotted) and pump parameters of $r=0.0167\gamma$ (solid); 0.0178γ (dashed); 0.0307γ (dotted).

Here we have to distinguish two cases: If we have a large constant pump rate and vary the probe-field amplitude, then the susceptibility shows the behavior plotted in Fig. 4. In this case there is only a particular value of the detuning for which the absorption is zero and we have gain in a certain region of the spectrum.

In the other case (see Fig. 5), we adjust the pump parameter to make χ'' touch the x axis, which could be realized in practice by a feedback control. This is in fact the more favorable case, since it results in a spectral region instead of a well-defined frequency where the absorption is very small. So in this case we are not restricted to monochromatic light as in all other cases but can use pulsed light. The intensity limit for this second case is estimated to be

$$\frac{|\Omega|}{\gamma}\chi' \lesssim 5\times 10^{-17} N \text{ cm}^3 . \tag{55}$$

The price we have to pay here is the relatively small value of the maximum field amplitude allowed to maintain a χ' of 10^{-5} in a gas of density $N=2\times 10^{22}$ m^{-3}. Again taking the parameter values of the example in Sec. II A, we have found $E \lesssim 10^7$ V m^{-1}.

At the point of zero absorption we have an increase of χ' with increasing field. This feature distinguishes the Raman from the other two schemes discussed and is the reason for the self-focusing in the Raman scheme in contrast to self-defocusing in the other schemes, as shall be discussed in the following section.

III. SELF-FOCUSING

Due to the dependence of the index of refraction on the intensity of the probe field in a nonlinear medium, the phase velocity in a beam with a radial profile changes with the distance from the center of the beam. The beam can therefore be focused or defocused depending on the sign of the Kerr coefficient n_2, which is defined as the coefficient of the first nonlinear correction to the index of refraction

$$n(E)=n_0+n_2|E|^2+n_4|E|^4+\cdots . \tag{56}$$

Self-focusing ultimately leads to an intense focus after a certain optical length which eventually may break down or ionize the medium.

At a point of zero absorption [$\chi''(E)=0$] the index of refraction can be written as

$$\begin{aligned} n(E)&=(1+\chi'^{(1)}+\chi'^{(3)}|E|^2+\chi'^{(5)}|E|^4+\cdots)^{1/2} \\ &\simeq n_0+\frac{\chi'^{(3)}}{2n_0}|E|^2 \\ &\quad+\frac{1}{2n_0}\left[\chi'^{(5)}-\left[\frac{\chi'^{(3)}}{2n_0}\right]^2\right]|E|^4+\cdots . \end{aligned} \tag{57}$$

Self-focusing occurs for an incidentally convergent Gaussian beam if $n_2=\chi'^{(3)}/(2n_0)>0$ and the field amplitude $|E|$ exceeds the critical value [15]

$$|E_{\text{crit}}|=\frac{\lambda}{2\pi d\sqrt{n_0 n_2}} , \tag{58}$$

where d is the beam radius at the entrance plane of the medium. In this case the focusing due to the optical Kerr effect is larger than the defocusing due to beam diffraction. A negative value of n_2 corresponds to self-defocusing. As we have seen from the solutions for the nonlinear susceptibility, the nonlinearities lead to a decrease of χ' at the point of zero absorption for the initial coherence and the microwave driven Λ schemes. This is equivalent to a negative n_2, i.e., to self-defocusing.

In the Raman scheme, this is not true in general. As we have shown, for certain parameter combinations there can be an increase of χ' at the point of zero absorption with increasing field amplitude. (Note, however, that the maximum value of χ' always decreases with increasing field amplitude.) As the Raman scheme seems to be the most favorable for applications, we discuss this in detail.

The third-order susceptibility $\chi'^{(3)}$ for this scheme can be obtained by solving the equations of motion (45)–(54) using a perturbative method, i.e., by calculating the polarizations ρ_{ab} and $\rho_{ab'}$ separately to first and third order in E. The resulting $\chi'^{(3)}$ is plotted as a function of the detuning in Fig. 6. The regions where $\chi'^{(3)}$ is negative correspond to self-defocusing. The point of zero absorption with $\chi'>0$, however, shows a positive $\chi'^{(3)}$, i.e., self-focusing. As a numerical example we consider the case in Fig. 6. The point of zero absorption is at $\Delta=-1.67\gamma$,

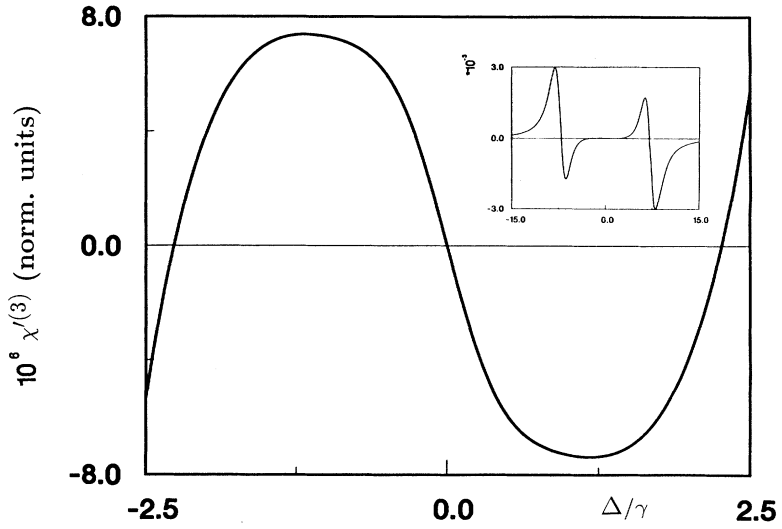

FIG. 6. Self-focusing data for the Raman scheme. Plotted is $\chi'^{(3)}[N\wp^4/(\epsilon_0\hbar^3\gamma^3)]^{-1}$ as a function of the detuning. The atomic parameters are chosen according to Fig. 5 (solid curve). The inset shows the surrounding spectral region.

and $\chi'^{(3)}$ takes the value $\chi'^{(3)}=6.4\times10^{-6}N\wp^4/(\epsilon_0\hbar^3\gamma^3)$. For the parameters used earlier ($\lambda=500$ nm, $\gamma=10^8$ s^{-1}, $N=2\times10^{22}$ m^{-3}) this gives with $d=0.1$ mm the extremely small critical field amplitude $E_{\text{crit}}=15$ V m^{-1}.

The Kerr coefficient in this case is $n_2\simeq10^{-8}$ V^{-2} m^2, which exceeds that of a conventional Kerr-type material such as CS_2 with $n_2\simeq10^{-21}$ V^{-2} m^2 by 13 orders of magnitude. It should be noted, however, that the Kerr coefficient is sufficient for the description of the nonlinear properties of the medium only if the next term of the expansion (57) is sufficiently small. This implies an upper bound for the field intensity

$$|E|^2 \ll \frac{\chi'^{(3)}}{\chi'^{(5)}-\left[\dfrac{\chi'^{(3)}}{2n_0}\right]^2} . \tag{59}$$

If the field intensity exceeds this value a numerical analysis of the full nonlinear case has to be used for an accurate description of the probe-field propagation.

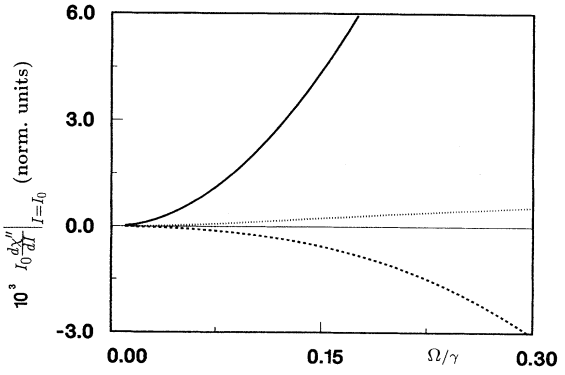

FIG. 7. Stability for the initial coherence scheme $I_0 d\chi''/dI|_{I=I_0}$ in normalized units as a function of the field amplitude. Plotted is $I_0 d\chi''/dI|_{I=I_0}[N\wp^2/(\epsilon_0\hbar\gamma)]^{-1}$. Parameters are $\gamma_a=\gamma_b=\gamma_{b'}=\omega_{b'b}=\gamma$ with $\rho^0_{aa}=0.4$, $\rho^0_{bb}=\rho^0_{b'b'}=\rho^0_{b'b}=0.3$ for the solid curve and $\rho^0_{aa}=0.2$, $\rho^0_{bb}=\rho^0_{b'b'}=-\rho^0_{b'b}=0.4$ for the dashed curve. For parameters for the dotted curve, cf. Fig. 2.

IV. STABILITY OF THE SOLUTIONS AGAINST INTENSITY FLUCTUATIONS

A closer inspection of Figs. 2(b) and 3(b) shows that changes of the input intensity may shift the point of vanishing absorption. This shift of the detuning of zero absorption can lead to an instability. For example, if we had fixed the field frequency at a point where we have zero absorption in the linear case (such as point A in Fig. 3), we see that an increase in the intensity leads to a negative χ'' at this point, i.e., to gain. Hence an initially small intensity fluctuation will be amplified which means that the system is unstable.

For a quantitative analysis, we start with the propagation equation of the probe-field intensity

$$\frac{dI}{dz}=-\frac{1}{\lambda}\chi''I . \tag{60}$$

Suppose we have chosen the parameters in such a way that for a given mean input intensity I_0, $\chi''(I_0)=0$. If there are some fluctuations of the input intensity around this value, so that $I=I_0+\delta I$, we have

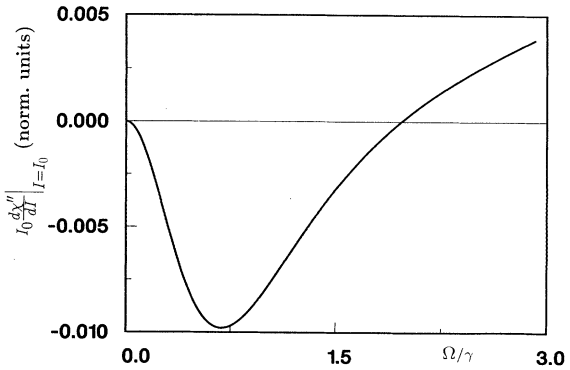

FIG. 8. Stability for the microwave scheme. Plotted is the same quantity as in Fig. 7. Parameters are $\gamma_c=0.1\gamma$, $\Omega_\mu=r_c=\gamma$, $\gamma_\mu=r=0$.

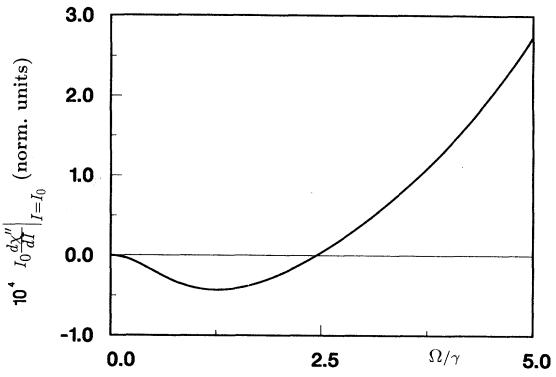

FIG. 9. Stability for the Raman scheme in a case with well-defined zero of absorption. Plotted is the same quantity as in Fig. 7. Parameters are $\Omega_R=5\gamma$, $r=0.2\gamma$. Atomic parameters are chosen according Fig. 5.

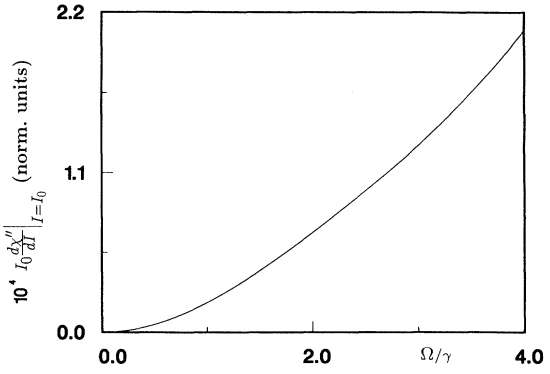

FIG. 10. Stability for the Raman scheme in a case with spectral region of small absorption. Plotted is the same quantity as in Fig. 7. Parameters are $\Omega_R=10\gamma$, $r\simeq 0.03\gamma$ (adjusted to the field amplitude). Atomic parameters are chosen according to Fig. 5.

$$\frac{d(\delta I)}{dz}=-\frac{1}{\lambda}\left[I_0\frac{d\chi''}{dI}(I_0)\right]\delta I\equiv-\frac{1}{\lambda}\alpha\delta I\ , \tag{61}$$

from which we find

$$\delta I(z)=\delta I(z=0)\exp\left[-\alpha\frac{z}{\lambda}\right]\ . \tag{62}$$

Thus the sign of the coefficient α determines the stability of the system. As an example we show the results for different schemes and parameter ranges in Figs. 7–10.

α can be derived from the analytic solutions of Sec. II in each specific case. Because of the large number of free parameters it is not possible to give a simple general criterion for stability. It is worth noting, however, that the Raman scheme under conditions leading to a susceptibility spectrum as in Fig. 5 is always stable.

The considerations of this section are important for possible applications, as the following example shows for the case of traveling fields: We choose the parameters as used in Fig. 8. For a field amplitude of $\Omega=\gamma$, we get $\alpha\sim-1$. This means that after traveling a distance of $n\lambda$, an intensity fluctuation will be amplified by a factor of e^n.

V. SUMMARY

In the present paper we obtained the nonlinear electric susceptibilities for three different coherence-establishing schemes. For two of them, the initial coherence and the microwave scheme, analytic expressions were given. The results show a limit for the cw field amplitude for a given index of refraction and a given atomic density that touches the region of the field amplitudes necessary for the laser accelerator.

Our results for the nonlinearities in the susceptibility show that strong self-focusing or self-defocusing may show up for high field intensities and that these effects must be taken into account already for small field amplitudes.

Another feature that was not possible to investigate in the linear calculations is the instability against intensity fluctuations. The analysis shows that severe instabilities can arise. The general dependence of the stability on the system parameters is, however, very complicated and remains to be investigated for each particular case.

ACKNOWLEDGMENTS

This work was supported by the Office of Naval Research. One of us (U.R.) is indebted to the "Studienstiftung des Deutschen Volkes" for support.

[1] G. Alzetta, A. Gozzini, L. Moi, and G. Orriols, Nuovo Cimento **36B**, 5 (1976); G. Alzetta, in *Coherence in Spectroscopy and Modern Physics,* edited by F. T. Arecchi, R. Bonifacio, and M. O. Scully (Plenum, New York, 1978); G. Alzetta, L. Moi, and G. Orriols, Nuovo Cimento **52B**, 209 (1979).

[2] H. R. Gray, R. M. Whitley, and C. R. Stroud, Jr., Opt. Lett. **3**, 218 (1978).

[3] K.-J. Boller, A. Imamoğlu, and S. E. Harris, Phys. Rev. Lett. **66**, 2593 (1991); J. E. Field, K. H. Hahn, and S. E. Harris, *ibid.* **67**, 3062 (1991).

[4] O. A. Kocharovskaya and Ya. I. Khanin, Pis'ma Zh. Eksp. Teor. Fiz. **48**, 581 (1988) [JETP Lett. **48**, 630 (1988)]; O. Kocharovskaya and P. Mandel, Phys. Rev. A **42**, 523 (1990); O. Kocharovskaya, R.-D. Li, and P. Mandel, Opt. Commun. **77**, 215 (1990); O. A. Kocharovskaya, F. Mauri, and E. Arimondo, *ibid.* **84**, 393 (1991); O. Kocharovskaya, P. Mandel, and Y. V. Radeonychev, Phys. Rev. A **45**, 1997 (1992).

[5] S. E. Harris, Phys. Rev. Lett. **62**, 1033 (1989); A.

Imamoğlu and S. E. Harris, Opt. Lett. **14**, 1344 (1989); A. Imamoğlu, Phys. Rev. A **40**, 2835 (1989); A. Imamoğlu, J. E. Field, and S. E. Harris, Phys. Rev. Lett. **66**, 1154 (1991).

[6] M. O. Scully, S.-Y. Zhu, and A. Gavrielides, Phys. Rev. Lett. **62**, 2813 (1989); L. M. Narducci, H. M. Doss, P. Ru, M. O. Scully, S.-Y. Zhu, and C. Keitel, Opt. Commun. **81**, 379 (1991); M. O. Scully, S.-Y. Zhu, L. Narducci, and H. Fearn, *ibid.* **88**, 240 (1992).

[7] S. Basile and P. Lambropoulos, Opt. Commun. **78**, 163 (1990).

[8] M. O. Scully, Phys. Rev. Lett. **67**, 1855 (1991).

[9] M. O. Scully and S.-Y. Zhu, Opt. Commun. **87**, 134 (1992).

[10] M. Fleischhauer, C. H. Keitel, M. O. Scully, and C. Su, Opt. Commun. **87**, 109 (1992).

[11] M. Fleischhauer, C. H. Keitel, M. O. Scully, C. Su, B. T. Ulrich, and S.-Y. Zhu, Phys. Rev. A **46**, 1468 (1992); A. D. Wilson-Gordon and H. Friedmann, Opt. Commun. **94**, 238 (1992).

[12] A third-order theory of noninversion lasers was given in S.-Y. Zhu and E. E. Fill, Phys. Rev. A **42**, 5684 (1990); M. O. Scully, S.-Y. Zhu, and H. Fearn, Z. Phys. D **22**, 471 (1992); S.-Y. Zhu, M. O. Scully, H. Fearn, and L. M. Narducci, *ibid.* **22**, 483 (1992); H. Fearn, M. O. Scully, S.-Y. Zhu, and M. Sargent III, *ibid.* **22**, 495 (1992).

[13] M. O. Scully, Appl. Phys. B **51**, 238 (1990); E. Bochove, G. Moore, M. O. Scully, and K. Wódkiewicz, in *Nonlinear Optics and Materials,* edited by C. D. Cantrell and C. M. Bowden [Proc. SPIE 1497, 338 (1991)].

[14] M. Sargent, M. O. Scully, and W. E. Lamb, *Laser Physics,* (Addison-Wesley, Reading, MA, 1974).

[15] Y. R. Shen, *The Principles of Nonlinear Optics* (Wiley Interscience, New York, 1984), p. 311.